Accepted Manuscript

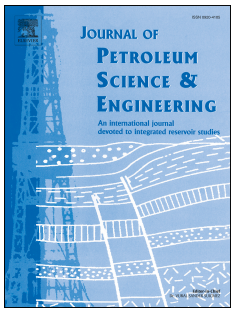

Comparison of sequential indicator simulation, object modelling and multiple-point statistics in reproducing channel geometries and continuity in 2D with two different spaced conditional data sets

Fengde Zhou, Daren Shields, Stephen Tyson, Joan Esterle

PII: S0920-4105(18)30229-8

DOI: 10.1016/j.petrol.2018.03.043

Reference: PETROL 4784

To appear in: *Journal of Petroleum Science and Engineering*

Received Date: 2 February 2016

Revised Date: 29 January 2018

Accepted Date: 8 March 2018

Please cite this article as: Zhou, F., Shields, D., Tyson, S., Esterle, J., Comparison of sequential indicator simulation, object modelling and multiple-point statistics in reproducing channel geometries and continuity in 2D with two different spaced conditional data sets, *Journal of Petroleum Science and Engineering* (2018), doi: 10.1016/j.petrol.2018.03.043.

Comparison of Sequential Indicator Simulation, Object Modelling and Multiple-point Statistics in Reproducing Channel Geometries and Continuity in 2D with Two Different Spaced Conditional Data Sets

Fengde Zhou [a,b], Daren Shields [a], Stephen Tyson [a,b,c], Joan Esterle [a,b]

[a] *School of Earth and Environmental Sciences, University of Queensland, Brisbane, Qld 4072, Australia*

[b] *Centre for Coal Seam Gas, University of Queensland, Brisbane, Qld 4072, Australia*

[c] *Universiti Teknologi Brunei, BE1410 Brunei Darussalam*

ABSTRACT

Fluvial sediments with multi-scale channels are difficult to model using classical two-point statistical methods, e.g. sequential indicator simulation (SIS) or object-based modelling (ObjM). Multiple-point statistics (MPS) has been used to generate facies, fracture and porosity distributions based on pattern statistics derived from training datasets. However, the ability of these three methods to reproduce channel geometry and continuity is not clear, especially when using differently spaced conditional data. This paper presents a case study to compare the application of these three methods in reproducing channels from a section of Amazon River based on two differently spaced conditional data sets. Results show that: the reproduction accuracy is similar between MPS and SIS; MPS provides the most connected channel facies (or most channel continuity) as compared to SIS and ObjM; and using a hand-

drawn facies based on the sampling points yield a similar accuracy to that achieved by using the reality facies distribution as the training image. Finally, we conclude that the application of MPS does not significantly increase the reproduction accuracy when compared to SIS channel models; however, MPS can generate realistic models with respect to channel geometry and continuity.

Keywords: Sequential indicator simulation; Object modelling; Multiple-point statistics; Channel geometry and continuity; Amazon River.

1. INTRODUCTION

Fluvial channels may be broadly classified on the basis of channel sinuosity and multiplicity into four-part taxonomy including straight, braided, meandering and anastomosing river systems (Rust, 1977; Miall, 2014). Individually, these channels can include up to 17 types of discrete lithologies grouped into 8 architectural elements (Miall, 2006). Due to the inherent complexity of these systems resulting in severe heterogeneity, channel systems have been the focus for many researchers (Chen et al., 2015).

In geological modelling, sequential indicator simulation (SIS) and object modelling (ObjM) are widely used to populate categorical variables such as facies, while multiple-point statistics (MPS) is used comparatively less due to its inherent complexity and practical limitations such as increased run time and practical issues such as (1) uncertainty in geological scenarios, (2) scanning template (or search mask) and non-stationarity (Strebelle and Zhang, 2004; Eskandari and Srinivasan, 2010), and (3) subjectively in training image selection (Strebelle, 2002). Stationarity, one of the main requisites for the construction of a valid training image, requires the mean and variance of a variable be constant throughout a model area. In reality, this is seldom the case for most geological systems at regional scales.

SIS populates properties using variogram models, which describe the change of linear correlation with increasing offset – a technique known as two-point geostatistics (Journel, 1983; Journel and Isaaks, 1984; Journel and Alabert, 1988; Deutsch, 2006). This method is most appropriate if (1) the shape of particular facies bodies is not clear (Pyrcz and Deutsch, 2014), or (2) with a high density of conditional data, e.g. with close well spacing or dense 3D seismic data (Zhou et al., 2016). Facies distributions generated by SIS can appear patchy or unstructured when unconstrained by secondary data (Deutsch, 2006). ObjM, also known as marked point process (Haldorsen and Chang, 1986; Haldorsen and MacDonald, 1987; Haldorsen and Damsleth, 1990; Holden et al., 1998) or Boolean simulation (Seifert and Jensen, 2000), populates facies based on pre-defined geometries (i.e., objects) rather than two-point geostatistics. Facies fraction, orientation, amplitude, wavelength, width, and thickness are some of the input parameters needed to define the objects for ObjM (Holden et al., 1998; Manzocchi et al., 2007; Stephen et al., 2001). MPS, a pixel-based sequential simulation algorithm, is capable of producing models with more geological complexity than SIS and better honours hard data than ObjM (Strebelle and Journel, 2001; Strebelle, 2002; Mariethoz et al., 2010; Rezaee et al., 2015). In particular, MPS generates models by rendering complex facies connectivity patterns which may be critical for the prediction of fluid flow and transport problems (Mariethoz et al., 2010). Applications of the algorithm have ranged from a simulation of a fluvial reservoir facies using different training images and nested sequences (Strebelle, 2002) to modelling porosity distributions in a carbonate reservoir (Zhang et al., 2006). MPS has also been used to generate facies and fracture distributions (Erzeybek et al., 2012; Peredo and Ortiz, 2012; Stuart et al., 2014). In practice, ObjM uses multiple iterations to place the geo-bodies into the 3D grid, and hence requires longer run-times to honour hard data as compared to either SIS or MPS (Caers, 2001; Strebelle and Journel, 2001; Strebelle, 2002; Caers and Zhang, 2004; Liu et al., 2004). Additionally, ObjM

may not honour all hard data, e.g. facies fraction or object geometries particularly with respect to datasets with an abundance of hard data.

To understand the difference between SIS, ObjM and MPS, Bastante et al. (2008) compared these three methods in modelling slate deposits. They concluded that the estimated useful slate percentages by MPS were much closer to reality than indicator Kriging (IK) or SIS but the results relied partly on information obtained via IK. Larriestra and Gomez (2010) compared SIS, ObjM and MPS for a high sinuosity fluvial system and concluded that channel probability modes were represented more realistically by MPS than other modelling techniques. De Iaco and Maggio (2011) compared the predicted spatial distribution of limestone by SIS and MPS and concluded that MPS better reproduced the spatial distribution of limestone and meandering channels. Though these three modelling methods have been tested, evaluated and compared in the oil and gas industry, comparing the effectiveness of SIS, ObjM and MPS in reproducing channel distribution with different spaced data has not been adequately covered in academia. While data spacing plays a critical role in geological modelling.

2. DATA AND METHODOLOGY

2.1. Data

This study focuses on one section of the Amazon River (Fig. 1a), located in Brazil near the Atlantic Ocean. An area of 80×80 km^2 was digitised and imported into Petrel^{TM} (Fig. 1b). Figures show that there are three distinct orders (scales) of channels which can be classified based on their unique depositional architectures, e.g. into primary, secondary and tertiary channels with widths of approximately 8 km, 3 km and 1 km, respectively. The areal fractions are 17.8%, 8.1% and 6.4% for primary, secondary and tertiary channels, respectively (Fig. 1b). The total areal fractions are 32.3% and 67.7% for channel and

floodplain respectively. In the following study, we combined primary, secondary and tertiary channels as one facies of channel in modelling because we have no training image for each of these channels.

Fig. 2 shows the sampled data points (used as model inputs) using two different spacings, e.g. 2.5 km and 5.0 km. Fig. 2a shows data points with sampling spacing of 2.5 km. We can see most points consist of primary channels and partial secondary channels, hence primary and secondary channels will be well represented in the model. If a sampling interval of 5.0 km is used, most sample points are from primary channels hence only the primary channel will be adequately represented in the models. The original fraction calculated from these data points was used as the target input statistic in the modelling process.

2.2. Methodology

The intent of this paper is to compare the ability of SIS, ObjM and MPS to reproduce channel geometry and continuity by assessing the reproduction accuracy and facies connectivity of models constructed with the various methods. Note that the accuracy in geomodelling is better measured by assessing the geological models by means of dynamic simulation, in which the behaviour of a static grid is interrogated by varying dynamic conditions. In this study, the reproduction accuracy means the ratio of cells, which have same facies as the given facies distribution, to the total cells in the model. The conditional data (hard data) were sampled based on the digitised facies distribution with two different spacings of 5.0 km and 2.5 km respectively.

The algorithms for SIS, ObjM and MPS are briefly described herein; however, for a more comprehensive background regarding the application of these three techniques readers are referred to Bastante et al. (2008). Table 1 presents the comparison of steps for these three methods.

The indicator approach used by SIS transforms facies into binary variables when dealing with categorical variables like facies (Falivene et al., 2006). SIS is based on indicator kriging which gives an estimation of relative proportions of the different facies. SIS generates a random sequential path for property population using a pseudo-random number generator that allows the user to enter a given seed values so that multiple stochastic runs are repeatable. Each other unknown location within a grid is sequentially visited and a value for the variable is estimated based on the predicted relative probabilities.

In ObjM, object facies were introduced to replace a background facies such as undifferentiated floodplain sediments or marine shales (Falivene et al., 2006). The geometric and dimensional ranges of the introduced object facies are defined to reproduce the variability of sedimentary elements in the depositional model (Haldorsen and Chang, 1986; Clementsen et al., 1990; Tyler et al., 1994; Deutsch and Wang, 1996; Deutsch and Tran, 2002). The algorithm begins by finding a point in the model which has the same facies code as the body; then makes a body for the given facies with its predefined geometry; then the body is located in the model to honour hard data. These processes iterated until the object facies proportions, which are generally considered as the most critical parameter (Falivene et al., 2006), are consistent with facies global fraction.

MPS is based on a stationary training image which can be generated using densely and regularly sampled field-data (Okabe and Blunt, 2005), photographs of outcrops or aerial photographs processed with a computer-aided design (CAD) algorithm, ObjM (Bastante et al., 2008) or hand-drawn models (Zhou et al., 2016). A training image is a 3D model defining the typical geometries and relationships that will be converted to conditional probability distributions known as a multi-point facies pattern. The training image is used to define the neighbourhood relationship of respective facies by creating patterns defined by probability distribution functions (pdf). During the pattern creation, multi-grids (Strebelle, 2002) are used

to describe both small and large-scale structures, similar to short and long variogram ranges if using two-point geostatistics (Okabe and Blunt, 2005; Xu et al., 2012). The multi-grids concept was initially proposed by Gómez-Hernández (1991) and Tran (1994). The multi-grids number and search radius are provided in an ellipsoid search mask to create the patterns. Using different multi-grid schemes yields different results (Comunian et al., 2012; Straubhaar and Malinverni, 2014). In MPS modelling, the digitised distribution of channels and floodplain in Fig. 1 is used as the training image. The MPS algorithm of SNESIM, introduced by Strebelle (2002), in Petrel^{TM} was used in MPS modelling.

Fig. 3a is a training image with a channel areal ratio of 26%. This area is gridded into 400 cells. According to the events' template with four neighbour conditioning data (Fig. 3b), the data event number is 2^4=16 (Fig. 3b); then we can account for the probability of each event globally as shown in Table 2. For example, there are 168 grids are cross-connected with four neighbouring grids at event #1 (EV1); 5 of those 168 grids are channel facies.

3. RESULTS AND DISCUSSION

3.1. Modelling results with data sampling space of 2.5 km

Based on a sampling space of 2.5 km, the input fraction of channels is 32.5% which is similar to the actual volume channel percentage of 32.3%. In order to use SIS, we first analyse the horizontal indicator variogram using a maximum search distance in x- and y-direction of 60 km and a lag distance of 10 km. Fig. 4a shows the generated horizontal variogram map which indicates a major orientation of about 45˚. We then generated the directional variogram along major and minor orientation respectively. The lag distance is 2 km and the number of lags is 30 for both major and minor orientation. The band-width is 2.5 km; tolerance angle is 45˚; lag tolerance is 50%. Fig. 4b and 4c show the experimental standardised semivariance (Zhou et al., 2015) and its regressions. Results show that the sill is

1.08 and major and minor ranges are 16.2 km and 7.4 km respectively. The major and minor ranges from indicators are similar to the maximum width and length of the channel facies (Guo and Deutsch, 2010).

SIS is used to generate the facies distributions as shown in Fig. 5 with nine realisations based on the results of variogram analysis. Results show that the primary channel polygons are filled with channels, reflecting the techniques generally high accuracy of reproducing primary channels; however, the secondary and tertiary channels are more difficult to reproduce because their major and minor orientations are not the same as the inputs. If the secondary and tertiary channels are given different facies codes, they can have different variograms with different orientations. Also, if the variogram model has nested structures the short-range structures can have different orientation and anisotropy to the longer structures. This study combined all the channels and the accuracies are quantified in section 3.3.

In ObjM input fractions and geometries, e.g. orientation, amplitude, wavelength, width, thickness, and trends for channels are defined a priori. Table 3 lists the modelling parameters used in which the channel orientation is taken from the variogram analysis while channel width is derived from the digitised statistics. The amplitude and wavelength are assumed as listed in Table 3 because they are difficult to be measured for the channels in Fig. 1. In ObjM, we selected honouring hard data as the honouring priority and Fig. 6 shows that ObjM struggles to honour all hard data. In addition, it is a time-consuming technique with approximately 3hrs required to generate 9 realisations compared to several minutes for equivalent SIS or MPS models. It is worth noting that changing the inputs, e.g. channel geometry, trends may improve the conditioning of hard data and modelling accuracy.

In MPS modelling, the digitised distribution of channels and floodplain in Fig. 1 is used as the training image. Ellipsoid search mask with a radius of 10 grid nodes and number of multi-grids of 3 is used to create the patterns. Note that the ellipsoid search mask defined in

Petrel™, which uses the SNESIM code, is quantified in nodes. In this study, the simulation grid size is same as the training image so no scaling is needed. Fig. 7 shows nine realisations which indicate a good match for the primary channel and significant characterisation of secondary and tertiary channels.

3.2. Modelling results with data sampling spacing of 5.0 km

With a sampling space of 5.0 km, the fraction of channels (the ratio of sampling points met with channel facies to the total number of sampling points) is 36.0%, which is higher than the actual value of 32.3% calculated from the digitised map. This result indicates that there is often a bias for the calculated fraction of channels from sampling points even with a regular data sampling spacing. In order to compare the results with the actual distributions as shown in Fig. 1b, a channel fraction of 32.3% was used to generate subsequent models. Fig. 8a shows that the horizontal variogram indicates a major range orientation of about 80˚. The major and minor ranges are 14.5 km and 11.8 km respectively (Figs. 8b and 8c), which indicate that the heterogeneity describing capacity decreases with the increase of sampling spacing. Note that the histogram of pairs suggests an inadequate sampling (non-homogenous) and the experimental variogram is distorted.

Fig. 9 shows the nine realisations of channel and floodplain distribution by SIS based on the sampled data with a spacing of 5.0 km. Results indicate that the estimated channel at right side matches well with the digitised image. The accuracy is higher than 90% for the largest channel in the right-hand image.

Fig. 10 shows the nine realisations of channel and floodplain distribution by MPS based on the sampled data with a spacing of 5.0 km. Results indicate that the estimated channels match well with the digitised image at some locations.

3.3. Accuracy comparison in reproducing channels

The accuracy, which is defined as the ratio of the matched grid number between estimations and the digitised image over the total number of grids, is used to compare the modelling results from different methods each with nine realisations. Based on the sampled data points with spacing of 2.5 km, the accuracy of SIS results ranges from 81% to 82% with an average of 81%; for MPS results, it ranges from 83% to 85% with an average of 84%; for ObjM results, it ranges from 57% to 65% with an average of 62%. Based on sampled data points with spacing of 5.0 km, the accuracy for SIS results ranges from 67% to 71% with an average of 70%; for MPS results, it ranges from 68% to 74% with an average of 71%. Note that the variogram for the floodplain is same as for the channels for a two facies model. The modelling results using the channel as the background facies are similar with those using floodplain as the background facies.

3.4. Comparison of channel connectivity

Journel et al. (1989) used a multiple step connectivity experiments to assess the geological modelling results. In this study, geometrical modelling is used to generate the distribution of connected volumes (bodies; Fig. 11). The probability of each connected volume is calculated based on the summation of juxtaposed grid blocks containing the channel facies code. Fig. 12 shows the cumulative probability for connected channels generated from SIS, ObjM and MPS based on sampled data with a spacing of 2.5 km. Results show that MPS has the greatest proportion of connected channels. Results show that the probability of the biggest connected channels ranges from 32% to 55% with an average of 45% by SIS; ranges of 43% to 61% with an average of 52% by ObjM; and ranges from 87% to 97% with an average of 92% by MPS. The probability of connected channels is 100% in Fig. 1b which indicates MPS results match well with reality. Note that assuming a complete set of

connected channel sands is hardly ever the case in a subsurface sedimentary record. Integration and representation of thin shale layers, their lateral extension and potential impact on flow behaviour are the challenges in the modelling of lobes and channel architecture (Falivene et al., 2006). Bastante et al. (2008) also reported that areas of slate by MPS are more regular and continuous than other methods.

Fig. 13 shows the cumulative probability of connected channels from SIS, ObjM and MPS based on sampled data with a spacing of 5.0 km. Results show that the probability of the biggest connected channels ranges from 30% to 78% with an average of 45% by SIS and ranges from 79% to 99% with an average of 89% by MPS. This indicates that the uncertainty increases with increasing data sampling spacing. Results by MPS match well with reality based on sampled data with a spacing of 5.0 km.

As reported by Caers and Zhang (2004), subsurface reservoir modelling is undertaken to produce models that accurately predict global flow properties while also estimating local recoverable grades of ore in mining. Therefore, the channel connectivity is an important factor on fluid flow and recoverable volumes. The connectivity in this study is quite simple which does not address more geological details, such as the relationships of connectivity with net: gross ratio and dynamic performance (Larue and Hovadik, 2006; Pranter, 2014).

3.5. Training image

Generating training images using densely and regularly sampled data (Okabe and Blunt, 2005), photographs of outcrops or aerial photographs processed with a computer-aided design (CAD) algorithm, ObjM and hand-drawn models may contradict the non-stationary requirement for training images. Image patterns, sourced from a training image, record the probability of each event (Zhou et al., 2016) regardless of the location of these events in the training image; hence MPS models cannot preserve the non-stationary features of the training

image (Strebelle and Zhang, 2004). Nested methods using several auxiliary variables, e.g. zones, distances, facies belt and rotation angles, as trend information were used to model non-stationary reservoir characteristics (Strebelle and Zhang, 2004; Yin et al., 2015), but the process requires known trends of the object property for locating the non-stationary reservoir characteristics.

Generating a training image by combining hard data and soft data from the whole object field will reduce the effect of non-stationary problems (Lorentzen et al., 2012). Figs. 14a and 13b show the processes to prepare a training image manually based on the sampled hard data with a spacing of 5.0 km and current direction and channel size. Note that the width of the secondary channel and the tertiary channel is assumed as 2.5 km and 1.0 km, respectively. Three steps are used in mapping channels; firstly, outline the primary channel according to the channel direction; then outline secondary channel which has similar flow trend as primary channel but also distribute between channels; the tertiary channel is outlined according to its width and flow direction of the primary and secondary channel. Facies are mapped based on the outline as shown in Fig. 14b then are converted into binary (categorical) facies, channel (including primary, secondary and tertiary channels) and floodplain. The distributed binary facies are used as training images for creating the MPS patterns.

Fig. 15 shows the simulated facies distribution with nine realisations. The accuracy of estimation of channels compared with reality ranges from 64% to 73% with an average of 69%. Results show that the accuracy is similar to that achieved by using the reality facies distribution as the training image.

4. CONCLUSIONS

In this study, a section of Amazon River is used to compare the application of SIS, ObjM and MPS in reproducing channels based on the digitised facies distribution in 2D with two different sampling spacing, 2.5 km and 5.0 km.

The reproducing accuracy by MPS is similar to that by SIS but higher than that by ObjM which was run with drilling data and channel orientation. Dense conditional data leads to high accuracy in reproducing facies distribution which means the harder data available to condition the simulations, the more deterministic the simulations become. MPS generated better-connected model than ObjM and SIS. Results by MPS match better with reality for the biggest connected channels than those produced by SIS and ObjM. However, generating a robust training image for MPS is still challenging in geological modelling. ObjM was used in generating the training images because it can well capture the shape and geometry of depositional bodies. This study shows that a manually generated training image yields a similar accuracy to that achieved by using real facies distribution as the training image.

ACKNOWLEDGEMENT

We acknowledge the Centre for Coal Seam Gas and its member companies (APLNG, Arrow Energy, QGC and Santos) for the support and Schlumberger for providing the license of Petrel™. We thank Helen Schultz for comments and corrections. We also thank the anonymous reviewers for providing the constructive comments.

REFERENCES

Bastante, F.G., Ordonez, C., Taboada, J., Matias, J.M., 2008. Comparison of indicator kriging, conditional indicator simulation and multiple-point statistics used to model slate deposits. *Engineering Geology* 98, 50-59.

Caers, J., Zhang, T., 2004. Multiple-point geostatistics: a quantitative vehicle for integrating geologic analogs into multiple reservoir models. In: Grammer, G. M., Harris, P. M., Eberli, G. P (Eds.). Integration of outcrop and modern analogs in reservoir modeling. *AAPG Memoir* 80, 383-394.

Chen, S., Lin, C., Liu, W., 2015. 3D geological modelling method of fluvial facies considering the information of sedimentary process. EJGE 20(6), 1487-1497.

Comunian, A., Renard, P., Straubhaar, J., 2012. 3D multiple-point statistics simulation using 2D training images. *Computers & Geosciences* 40, 49-65.

De Iaco, S., Maggio, S., 2011. Validation Techniques for Geological Patterns Simulations Based on Variogram and Multiple-Point Statistics. *Mathematical geosciences* 43, 483-500.

Deutsch, C.V., 2006. A sequential indicator simulation program for categorical variables with point and block data: BlockSIS. *Computers & Geosciences* 32, 1669-1681.

Deutsch, C.V., Journel, A.G., 1998. GSLIB Geostatistical Software Library and User's Guide. Second Edition.

Erzeybek, S., Srinivasan, S., Janson, X., 2012. Multiple-point statistics in a Non-gridded domain: Application to karst/fracture network modeling. *Quantitative Geology and Geostatistics* 17, 221-237.

Eskandari, K., Srinivasan, S., 2010. Reservoir Modelling of Complex Geological Systems--A Multiple-Point Perspective. *Journal of Canadian Petroleum Technology* 49, 59-68.

Falivene, O., Arbués, P., Gardiner, A., Pickup, G., Muñoz, J.A., Cabrera, L., 2006. Best practice stochastic facies modelling from a channel-fill turbidite sandstone analog (the Quarry outcrop, Eocene Ainsa basin, northeast Spain. AAPG Bulletin 90(7), 1003-1029.

Gómez-Hernández, J., 1991. A stochastic approach to the simulation of block fields' conductivity upon data measured at a smaller scale. *PhD thesis*, Stanford University, Stanford.

Guo, H., Deutsch, C.V., 2010. Fluvial channel size determination with indicator variograms. *Petroleum Geoscience* 16, 161-169.

Haldorsen, H.H., Chang, D.M., 1986. Notes on stochastic shales from outcrop to simulation models. In Reservoir Characterization, ed. Lake, L.W. and Carol, H.B., pp. 152-167. New York, USA: Academic.

Haldorsen, H.H., Damsleth, E., 1990. Stochastic modelling. Journal of Petroleum Technology 42(4), 404-412.Holden, L., Hauge, R., Skare, O., Skorstad, A., 1998. Modeling of fluvial reservoirs with object models. *Mathematical Geology* 30, 473-496.

Haldorsen, H.H., MacDonald, C.J., 1987. Stochastic modelling of underground reservoir facies (SMURF). SPE paper 16751 presented at the 62nd Annual Technical Conference and Exhibition held in Dallas, Texas.

Journel, A.G., 1983. Nonparametric estimation of spatial distribution. *Mathematical Geology* 15 (3), 445-468.

Journel, A.G., Alabert, F.G., 1988. Focusing on spatial connectivity of extreme valued attributes: stochastic indicator models of reservoir heterogeneities, SPE Paper 18324.

Journel, A.G., Isaaks, E.H., 1984. Conditional indicator simulation: application to a Saskatchewan uranium deposit. *Mathematical Geology* 16 (7), 685-718.

Journel, A.G., Journal, A.G., Alabert, F., 1989. Non-Gaussian data expansion in the Earth Sciences. *Terra nova* (Oxford, England) 1, 123-134.

Larue, D.K., Hovadik, J., 2006. Connectivity of channelized reservoirs: a modelling approach. Petroleum Geoscience 12, 291-308.

Larriestra, C.N., Gomez, H., 2010. Multiple-point simulation applied to uncertainty analysis of reservoirs related to high sinuosity fluvial systems: Mina EI Carmen Formation, San Jorge Gulf Basin, Argentina. AAPG International Conference and Exhibition, Rio de Janeiro, Brazil, November 15-18, 2009.

Liu, Y., Rusty Gilbert, A.H., Journel, A., 2004. A workflow for multiple-point geostatistical simulation. In Geostatistics Banff, eds. Leuangthong, O., Deutsch, C.V., pp. 245-254. Netherlands: Springer.

Lorentzen, R.J., Flornes, M., Naevdal, G., 2012. History matching channelized reservoirs using the Ensemble Kalman Filter. SPE Journal 17(1), 137-151.

Manzocchi, T., Walsh, J.J., Tomasso, M., Strand, J., Childs, C., Haughton, P.D.W., 2007. Static and dynamic connectivity in bed-scale models of faulted and unfaulted turbidites. In: Jolley, S.J., Barr, D., Walsh, J.J., Knipe, R.J. (eds) Structurally Complex Reservoirs, Geological Society, London, Special Publications, 292, 309-336.

Mariethoz, G., Renard, P., Straubhaar, J., 2010. The direct sampling method to perform multiple-point geostatistical simulations. Water Resources Research 46, W11536, doi:10.1029/2008WR007621.

Miall, A.D., 2014. Chapter 2: The facies and architecture of fluvial systems. In: Fluvial depositional systems. Springer Geology. Springer International Publishing Switzerland.

Miall, A.D., 2006. Reconstructing the architecture and sequence stratigraphy of the preserved fluvial record as a tool for reservoir development: a reality check. AAPG Bulletin 90(7), 989-1002.

Okabe, H., Blunt, M.J., 2005. Pore space reconstruction using multiple-point statistics. *Journal of Petroleum Science and Engineering* 46, 121-137.

Peredo, O., Ortiz, J.M., 2012. Multiple-point geostatistical simulation based on genetic algorithms implemented in a shared-memory supercomputer. *Quantitative Geology and Geostatistics* 17, 103-114.

Pranter, M.J., 2014. Fluvial architecture and connectivity of the Williams Fork Formation, Piceance Basin, Colorado: combining outcrop analogs and reservoir modelling for stratigraphic reservoir characterization. Search and Discovery Article #50959, presentation at Oklahoma City Geological Society, January, 2014, and Tulsa Geological Society, February 25, 2014.

Pyrcz, M.J., Deutsch, C.V., 2014. Geostatistical Reservoir Modeling, Oxford University Press, 2nd edition, USA, pp236.

Rezaee, H., Marcotte, D., Tahmasebi, P., Saucier, A., 2015. Multiple-point geostatistical simulation using enriched pattern databases. Stochastic Environmental Research and Risk Assessment 29, 893-913.

Rust, B.R, 1977. A Classification of Alluvial Channel Systems. Fluvial Sedimentology — Memoir 5, 187-198.

Seifert, D., Jensen, J.L., 2000. Object and pixel-based reservoir modeling of a braided fluvial reservoir. Mathematical Geology 32(5), 581-603.

Stephen, K.D., Clark, J.D., Gardiner, A.R., 2001. Outcrop-based stochastic modelling of turbidite amalgamation and its effects on hydrocarbon recovery. Petroleum Geoscience 7, 163-172.

Straubhaar, J., Malinverni, D., 2014. Addressing Conditioning Data in Multiple-Point Statistics Simulation Algorithms Based on a Multiple Grid Approach. *Mathematical geosciences* 46, 187-204.

Strebelle, S.B., 2002. Conditional simulation of complex geological structures using multiple-point statistics. *Mathematical Geology* 34, 1-21.

Strebelle, S.B., Journel, A.G., 2001. Reservoir modeling using multiple-point statistics. SPE paper 71324 presented at the SPE Annual Technical Conference and Exhibition held in New Orleans, Louisiana, 1–11.

Strebelle, S.B., Zhang, T., 2004. Non-stationary multiple-point geostatistical models. In: Leuangthong, O., Deutsch, C.V. (Eds.), Geostatistics Banff, 2004, 235-244.

Stuart, J., Moundney, N.P., McCaffrey, W.D., Lang, S., Collinson, J.D., 2014. Prediction of channel connective and fluvial style in the flood basin successions of the Upper Permian Rangal Coal Measures (Queensland). *AAPG Bulletin* 98(2), 191-212.

Tran, T., 1994. Improving variogram reproduction on dense simulation grids. *Computers & Geosciences* 20, 1161–1168.

Xu, Z., Teng, Q.Z., He, X.H., Yang, X.M., Li, Z.J., 2012. Multiple-point statistics method based on array structure for 3D reconstruction of Fontainebleau sandstone. *Journal of Petroleum Science and Engineering* 100, 71-80.

Yin, Y., Zhang, C., Li, S., 2015. A Location-Based Multiple Point Statistics Method: Modeling the Reservoir With Non-Stationary Characteristics. *AAPG Annual Convention and Exhibition*, Denver, CO., May 31 - June 3, 2015

Zhang, T., Bombarde, S., Strebelle, S.B., Oatney, E., 2006. 3D Porosity Modeling of a Carbonate Reservoir Using Continuous Multiple-Point Statistics Simulation. *SPE Journal* 11(3), 375-379.

Zhou, F., Shields, D., Tyson, S., Esterle, J., 2016. Nested approaches to modelling swamp and fluvial channel distribution in the Upper Juandah Member of the Walloon Coal Measures, Surat Basin. *The AAPEA Journal* 56, 81-100.

Zhou, F., Yao, G., Tyson, S., 2015. Impact of geological modelling processes on spatial coalbed methane resource estimation. *International Journal of Coal Geology* 146, 14-27.

Table 1. Comparison of workflows between SIS, ObjM and MPS.

SIS (Deutsch and Journel, 1998)	ObjM (Petrel, 2014)	MPS (Liu et al., 2004)
1. Establish grid system; 2. Assign data to the nearest grid node; 3. Build a random path through all of the grid nodes by seed number; 4. Search nearby data and previously simulated grid nodes; 5. Construct the conditional probabilities by Kriging; 6. Draw a value from conditional distribution; 7. Check results.	1. Find a point having the same facies code as the body; 2. Make a body with the given facies and geometry for the body; 3. Choose a random insertion point on the body; 4. Calculate the body thickness at the insertion point; 5. Search for that thickness among the upscalled wells still left to be honoured ; 6. Ensure that the body about to be inserted does not conflict with other upscalled cells; 7. If the body passes these checks, insert the body; 8. Loop from 2-7 until the global fraction is satisfied.	If no soft information is available, the steps are: 1. Scan training image to calculate the conditional probability, P(A|B), for facies A at data events B. P(A|B) is stored in the form of a tree called a multi-point facies pattern; 2. Define a random path to visit each unknown node u 3. Generate a probability for visiting node; 4. At location u, read B(u) with hard data plus previously simulated values; then retrieve conditional probability; P(A|B)(u) according to B(u); 5. Draw a value (facies) according to P(A|B)(u) and step (3) generated probability; 6. Repeat steps (3) to (5) till visited all unknown node.

Table 2. Statistic of global event probability and grid channel probability (Zhou et al., 2016).

Data event	Grid numbers		Event probability, %	Channel probability, %
	Channel	Floodplain		
EV1	5	163	42	3.0
EV2	5	9	3.5	35.7
EV3	7	16	5.75	30.4
EV4	10	4	3.5	71.4
EV5	3	19	13.6	9.1
EV6	0	0	0	0.0
EV7	6	0	1.5	100.0
EV8	30	37	16.75	44.8
EV9	26	43	17.25	37.7
EV10	1	0	0.25	100.0
EV11	1	2	0.75	33.3
EV12	5	0	1.25	100.0
EV13	2	1	0.75	66.7
EV14	3	1	1	75.0
EV15	0	0	0	0.0
EV16	1	0	0.25	100.0

Table 3. Parameters used in ObjM.

Parameters	Distribution	Min	Mean	Max
Orientation	Triangular	30˚	45˚	50 ˚
Amplitude	Triangular	6km	8km	10km
Wavelength	Triangular	10km	15km	20km
Width	Triangular	1.5km	7.4km	10km
Thickness	Not applicable because of 2D models were built			
Trends	Not used			

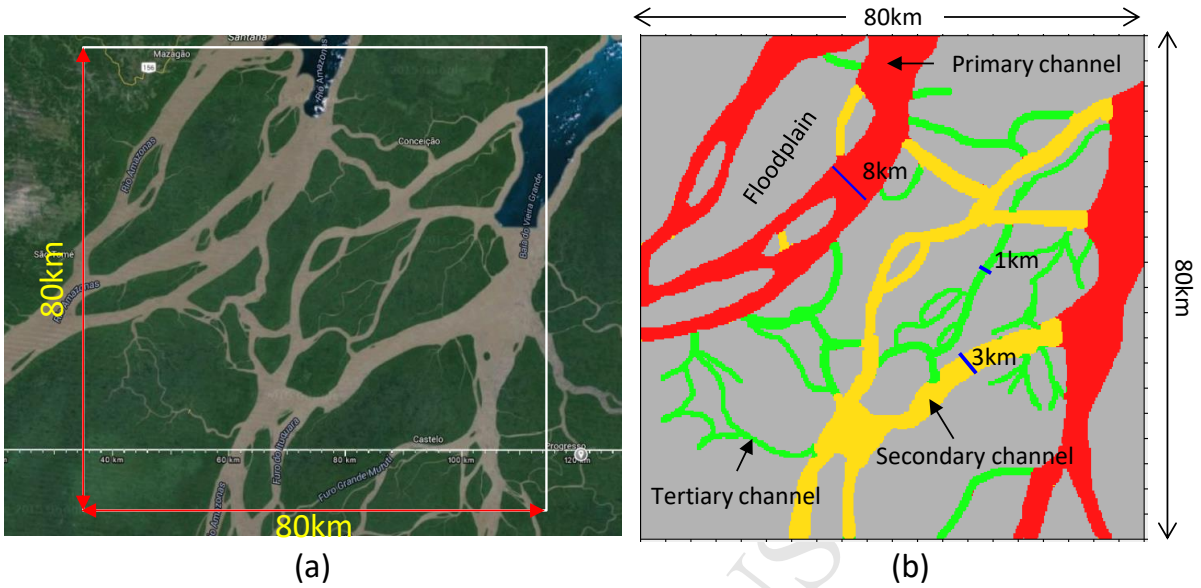

Fig. 1. Earth view of one section of Amazon River near Atlantic Ocean (a) and digitized channel and floodplain distribution (b). The location of study area is uploaded as an Interactive Map Data (KMZ). Note that the width of tertiary channel is enlarged in digitization and some small channels were ignored. The enlargement is help to visualize it in modelling.

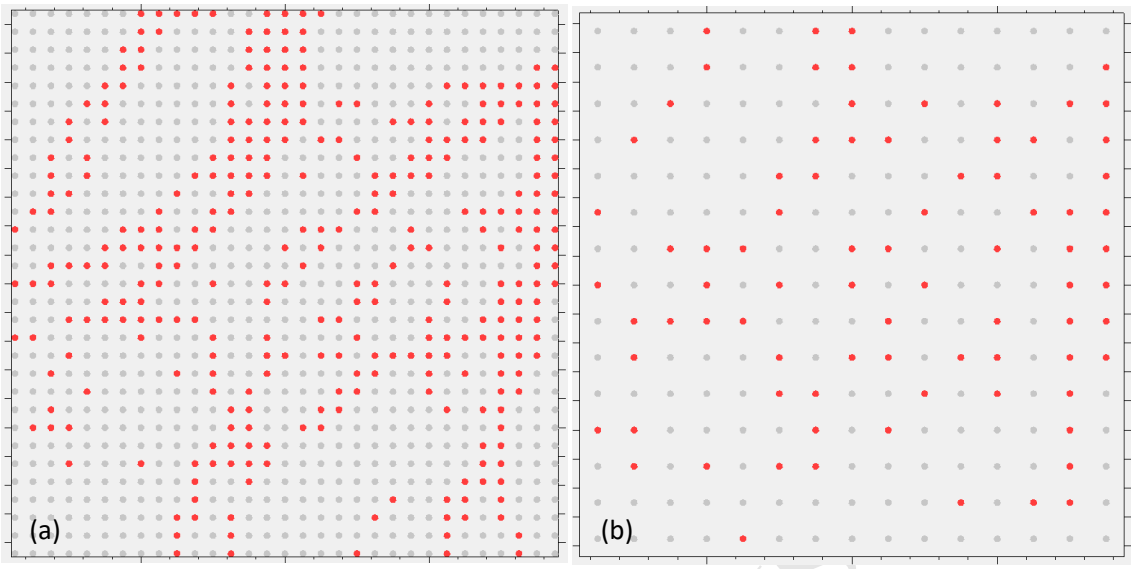

Fig. 2. Sampled data with spacing of 2.5 km (a) and 5.0 km (b). Red points were sampled from channel and grey points were sampled from floodplain.

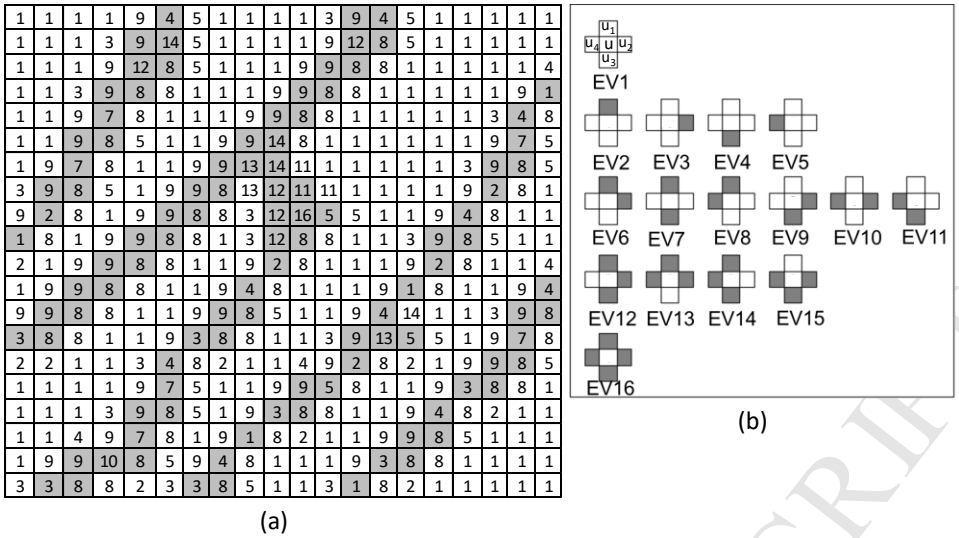

Fig. 3. A training image with marked event number (a) according to its 16 data events with four conditioning data (b) (Zhou et al., 2016). Filled grids=channel; blank=floodplain.

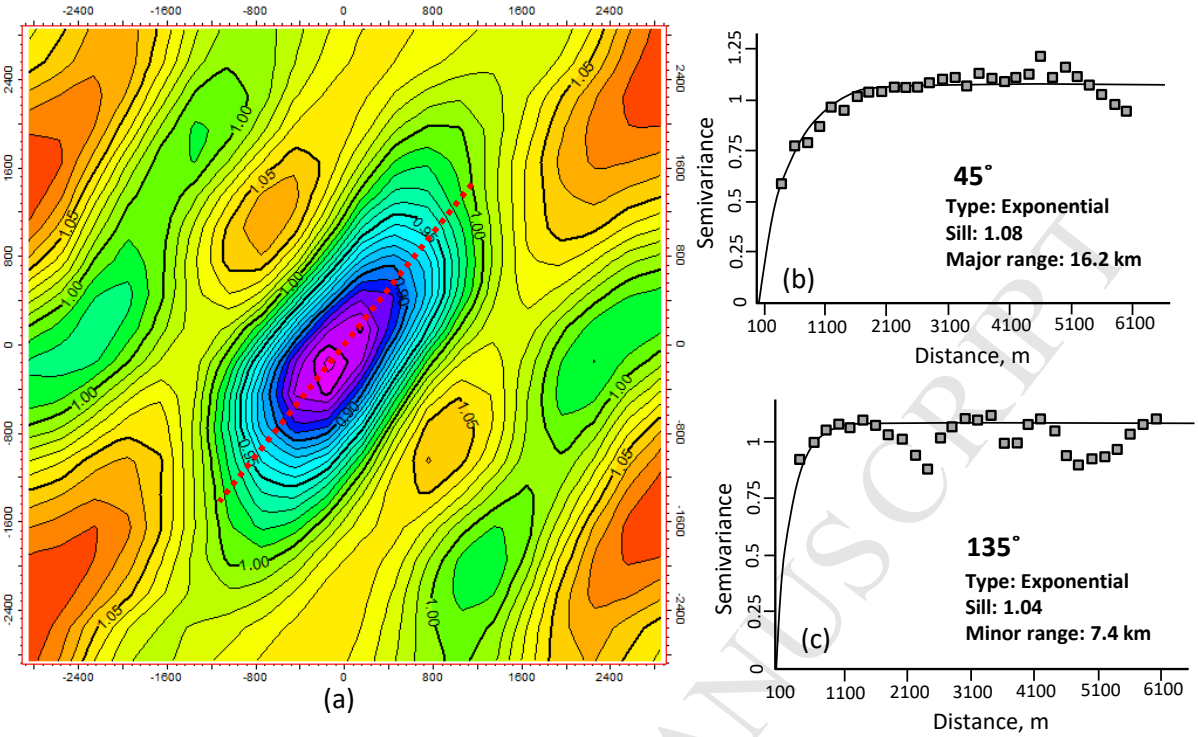

Fig. 4. Horizontal variogram (a), variogram along major direction (45˚; b) and variogram along minor direction (135˚; c). Note that the distance scale is 1:10 to reality.

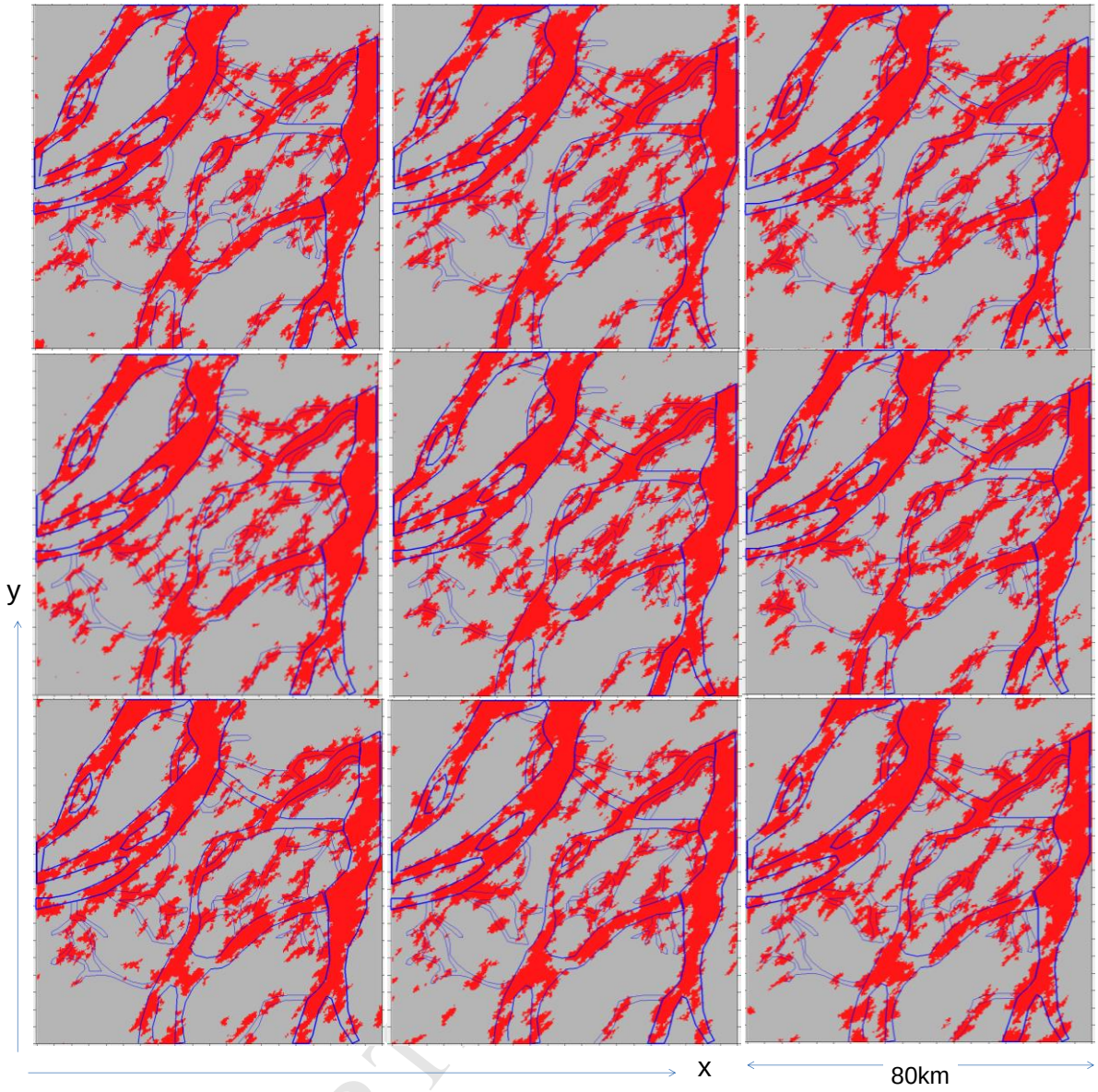

Fig. 5. Outlines of real channels overlap nine realisations of channel and floodplain distribution by SIS based on the sampled data with spacing of 2.5 km.

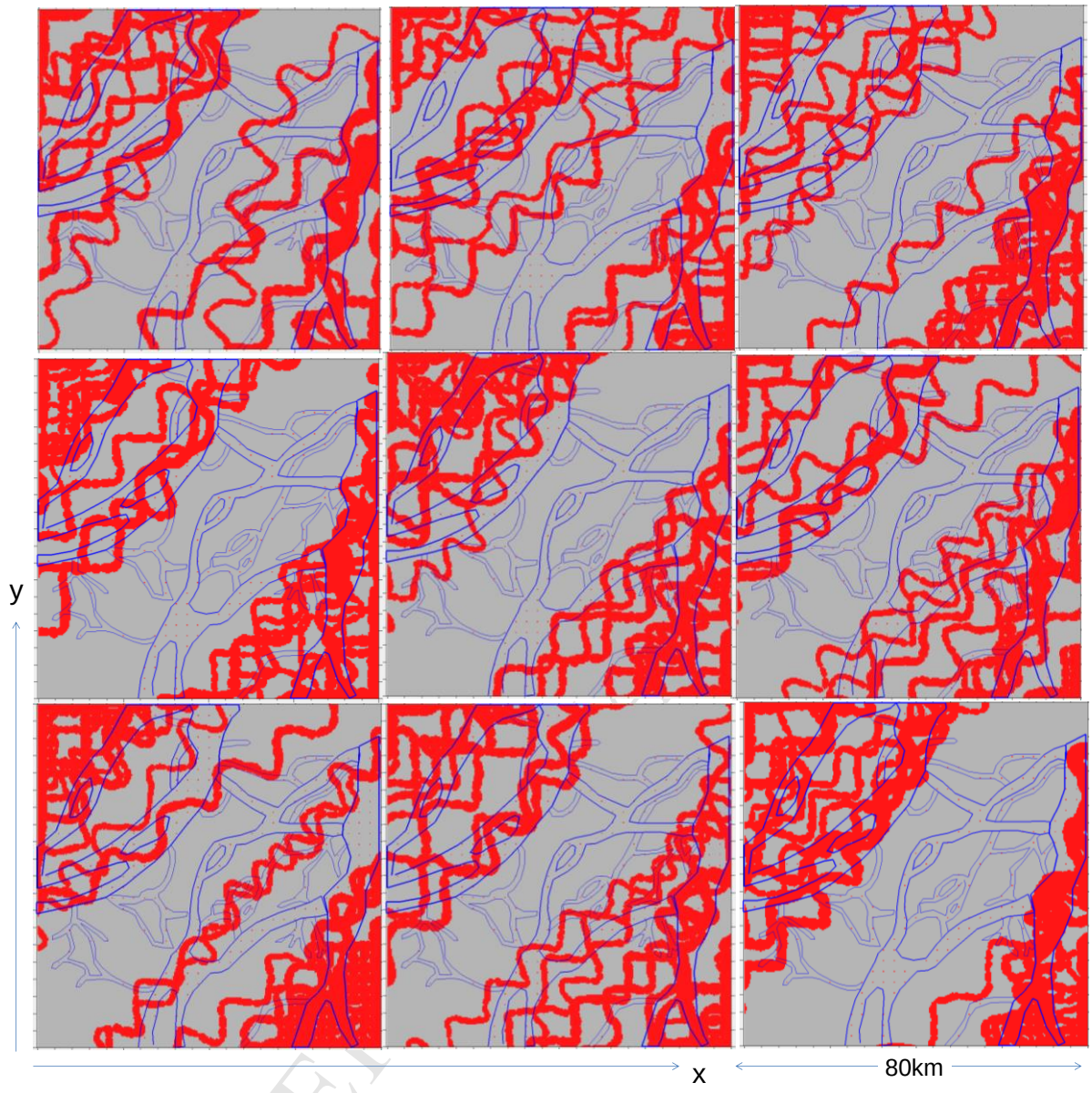

Fig. 6. Outlines of real channels overlap nine realisations of channel and floodplain distribution by ObjM based on the sampled data with spacing of 2.5 km.

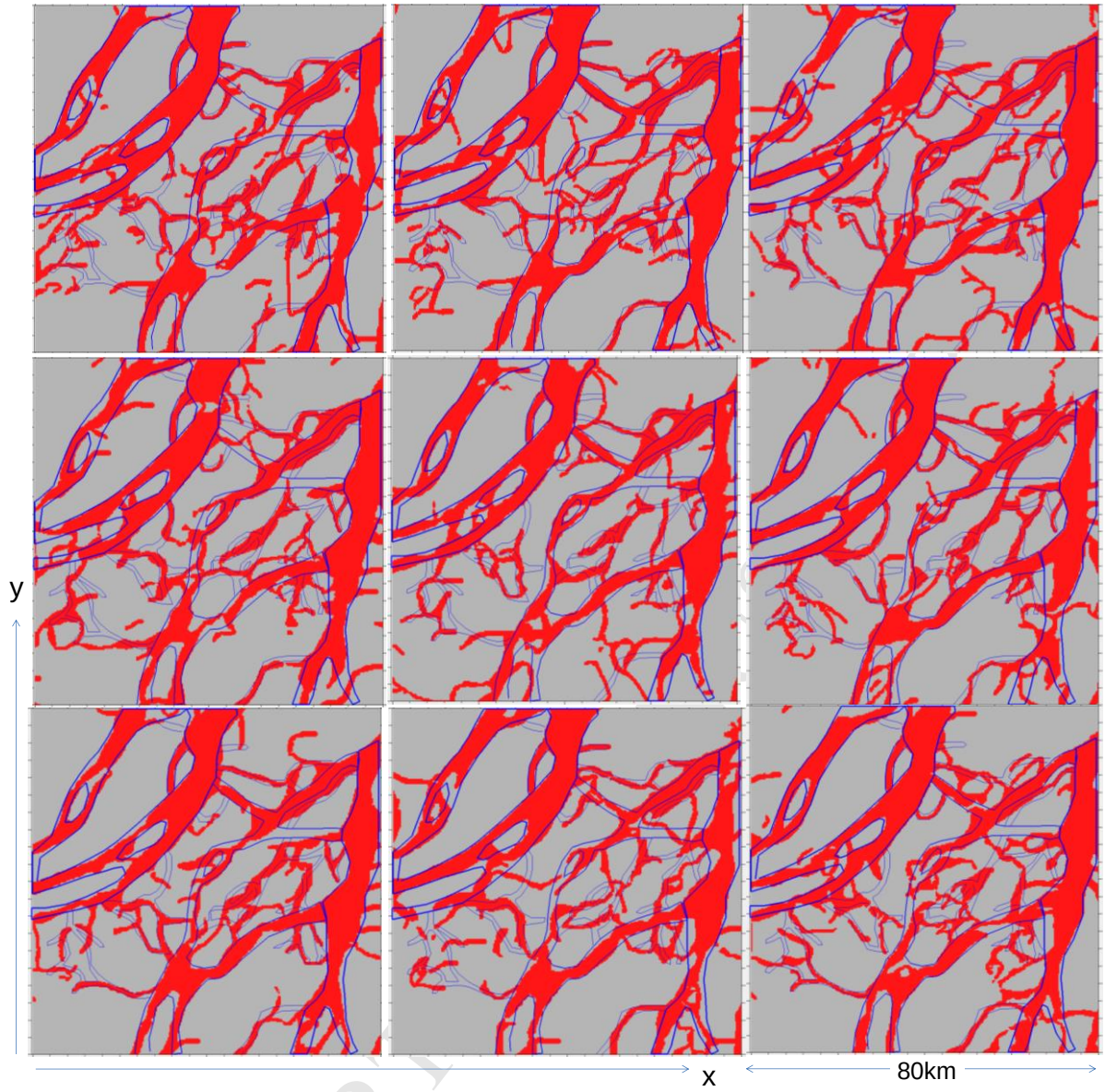

Fig. 7. Outlines of real channels overlap nine realisations of channel and floodplain distribution by MPS based on the sampled data with spacing of 2.5 km.

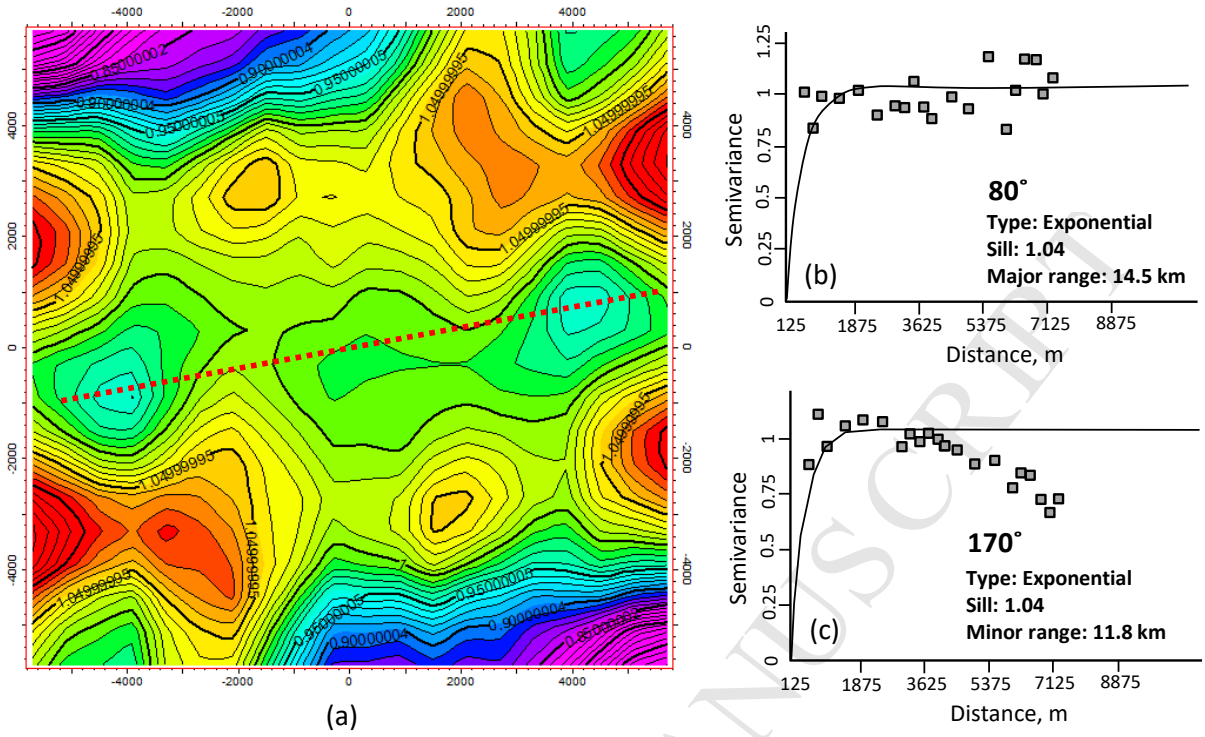

Fig. 8. Horizontal variogram (a), variogram along major direction (80˚; b) and variogram along minor direction (170˚; c) based on the sampled data with spacing of 5.0 km (Fig. 2b). Note that the map scale is 1:10 to reality.

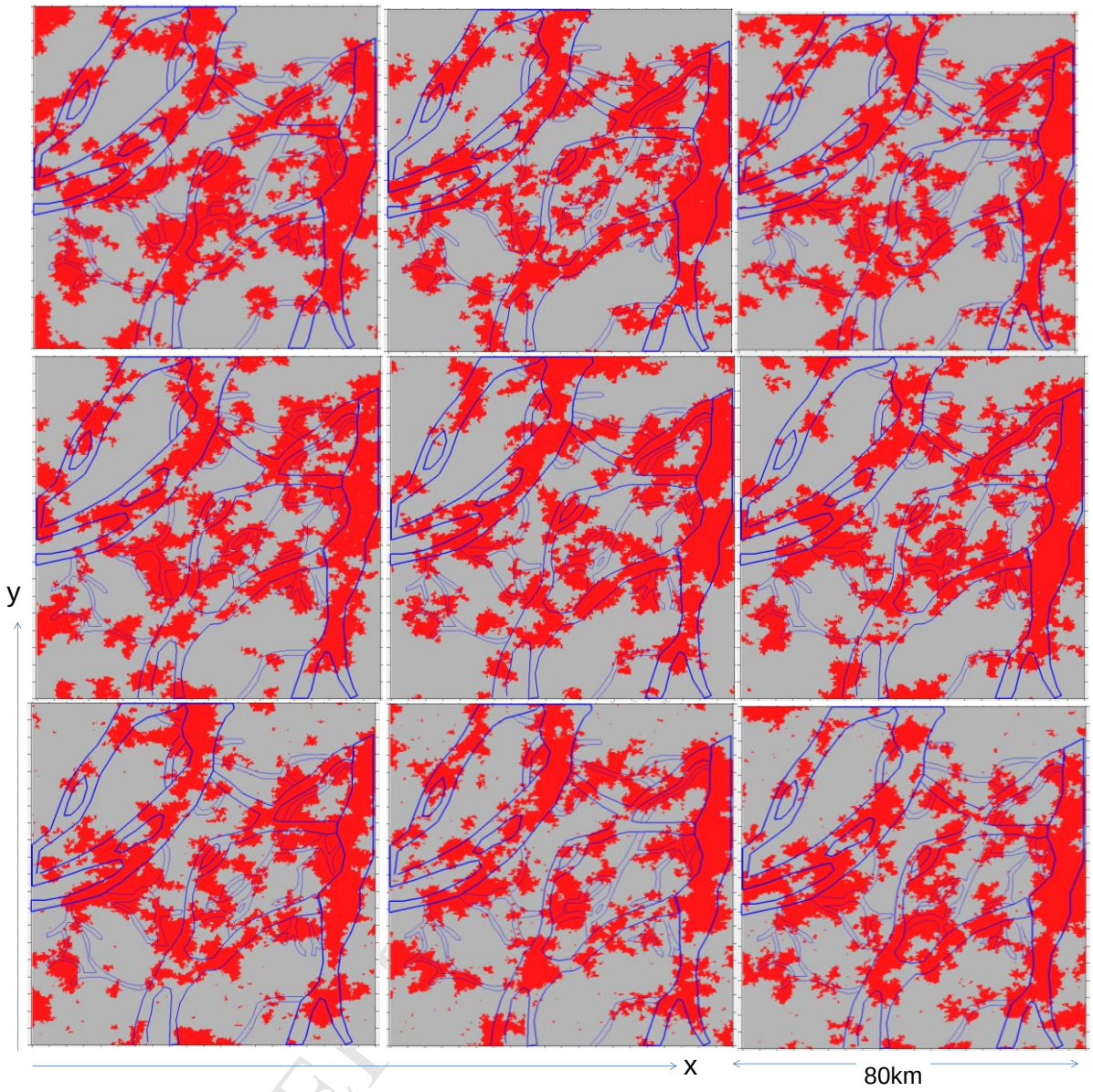

Fig. 9. Outlines of real channels overlap nine realisations of channel and floodplain distribution by SIS based on the sampled data with spacing of 5.0 km.

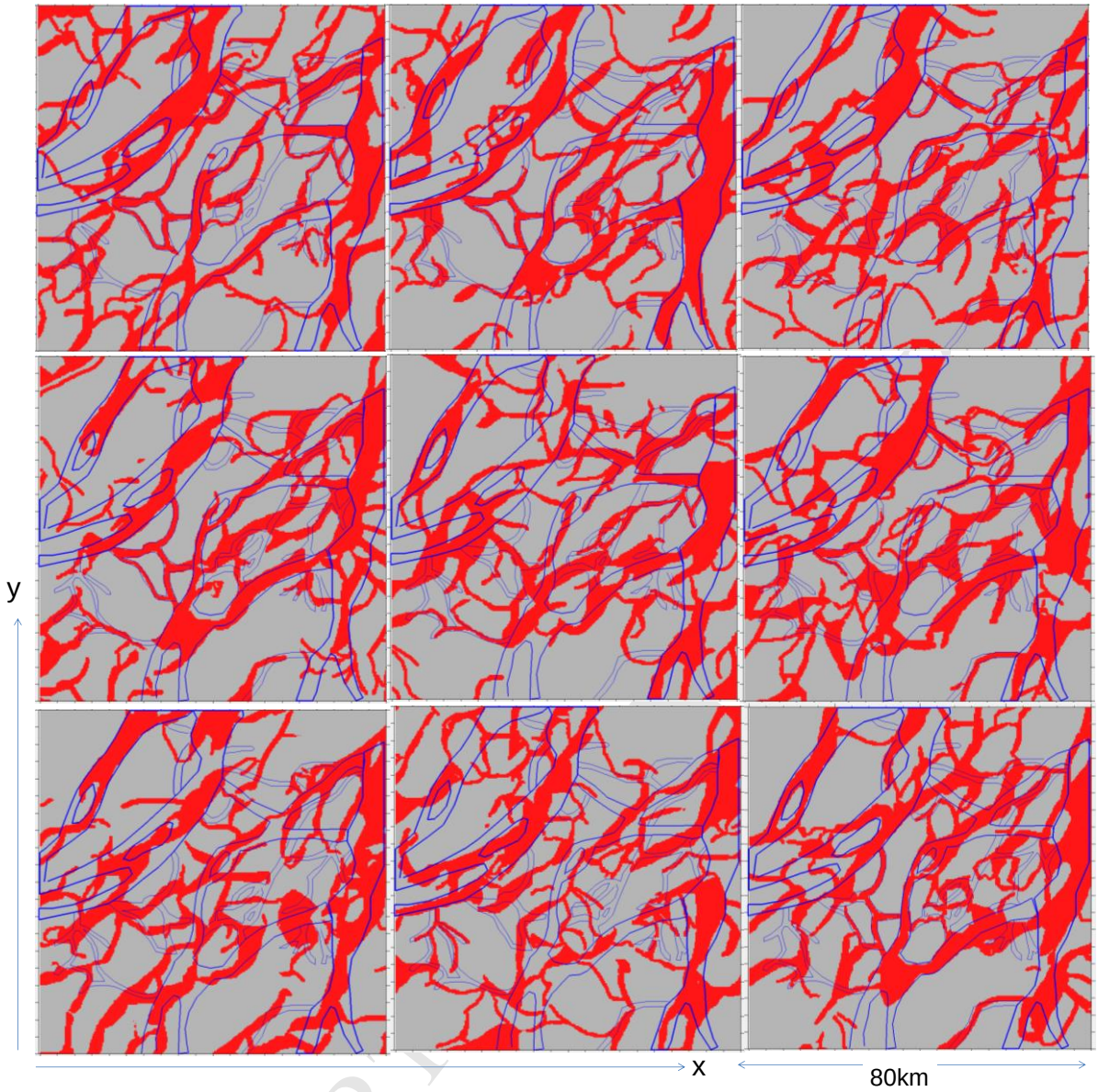

Fig. 10. Outlines of real channels overlap nine realisations of channel and floodplain distribution by MPS based on the sampled data with spacing of 5.0 km.

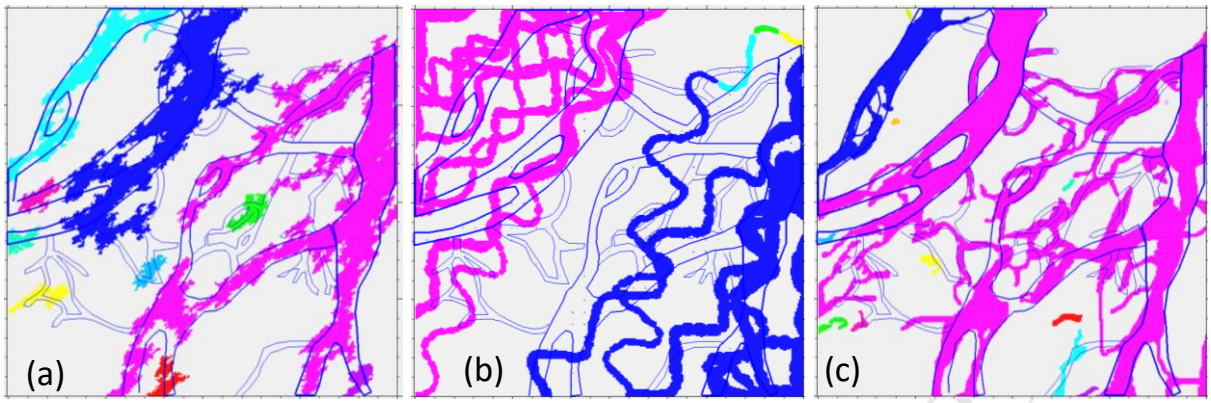

Fig. 11. Connected channels for realisation No.1 from SIS (a), ObjM (b) and MPS (c) based on sampled data with spacing of 2.5 km. Different colour represents different connected body.

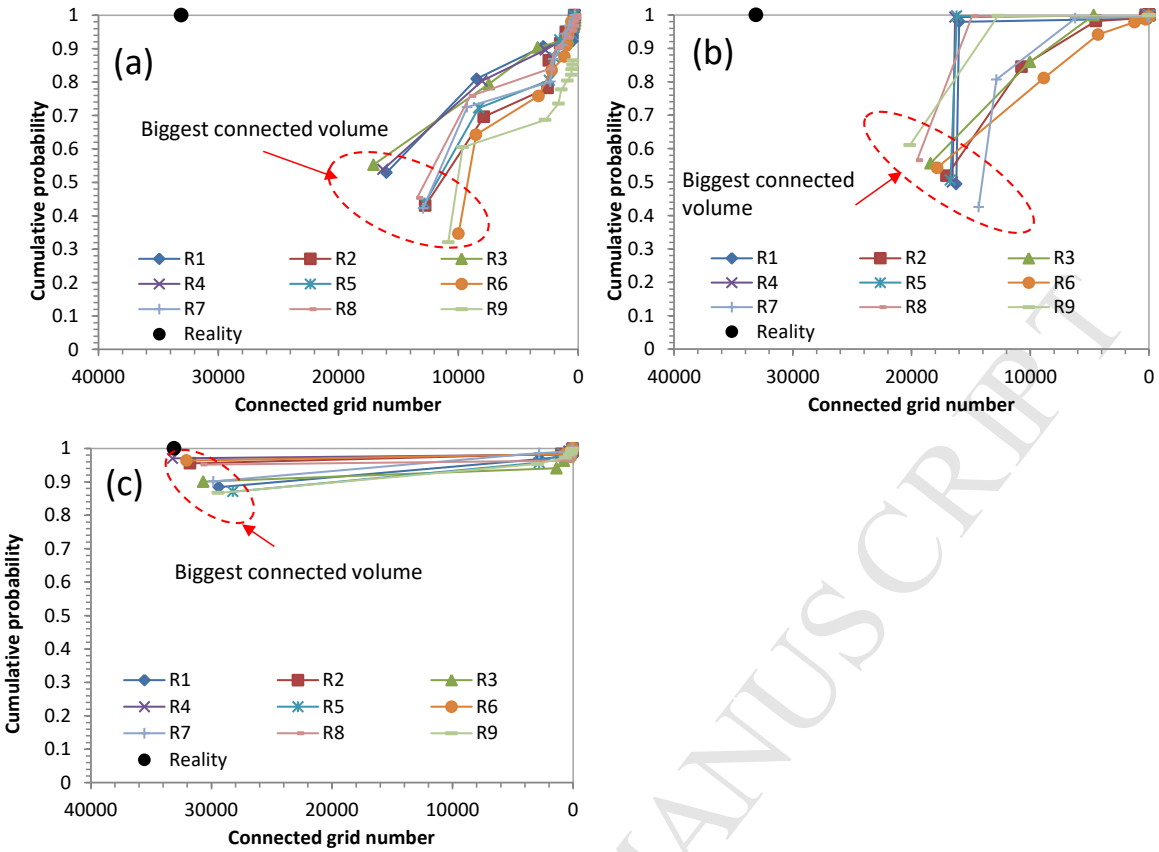

Fig. 12. Connected grid number of channels from SIS (a), ObjM (b) and MPS (c) based on sampled data with spacing of 2.5 km.

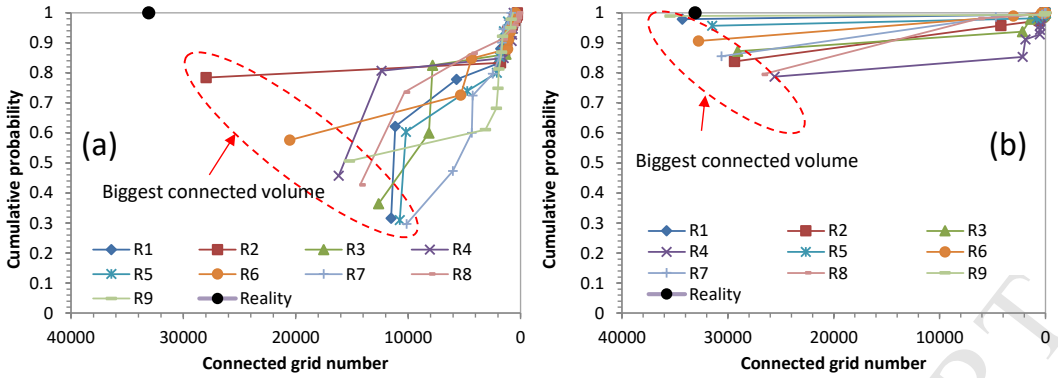

Fig. 13. Connected channels from SIS (a) and MPS (b) based on sampled data with spacing of 5.0 km.

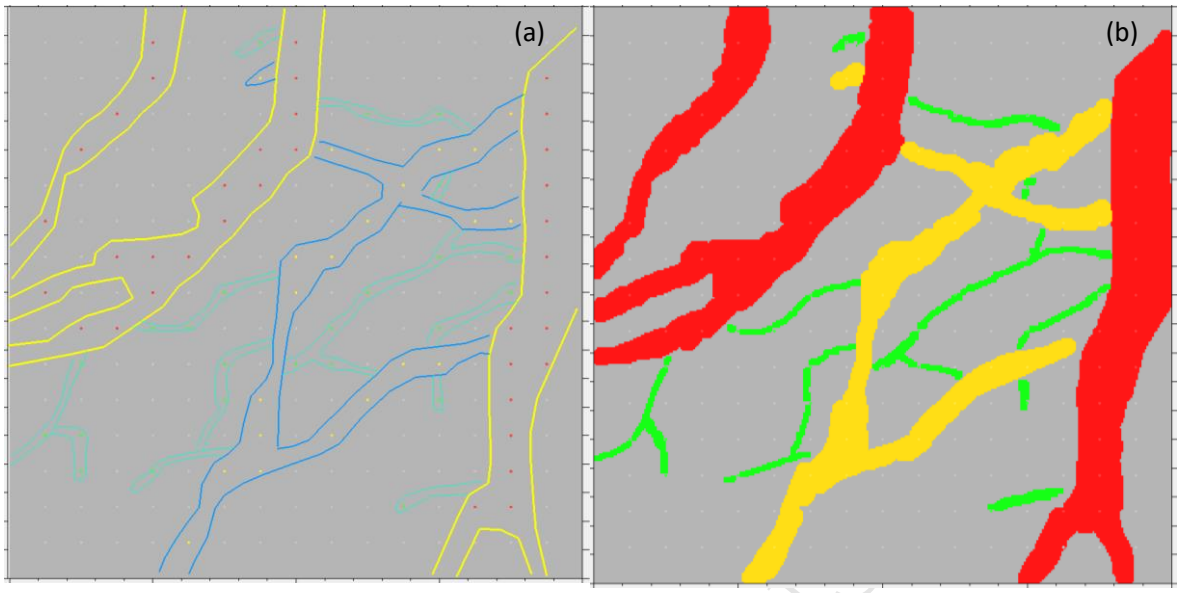

Fig. 14. Training image is prepared manually. (a) Channel outlines and (b) channel distribution filled manually.

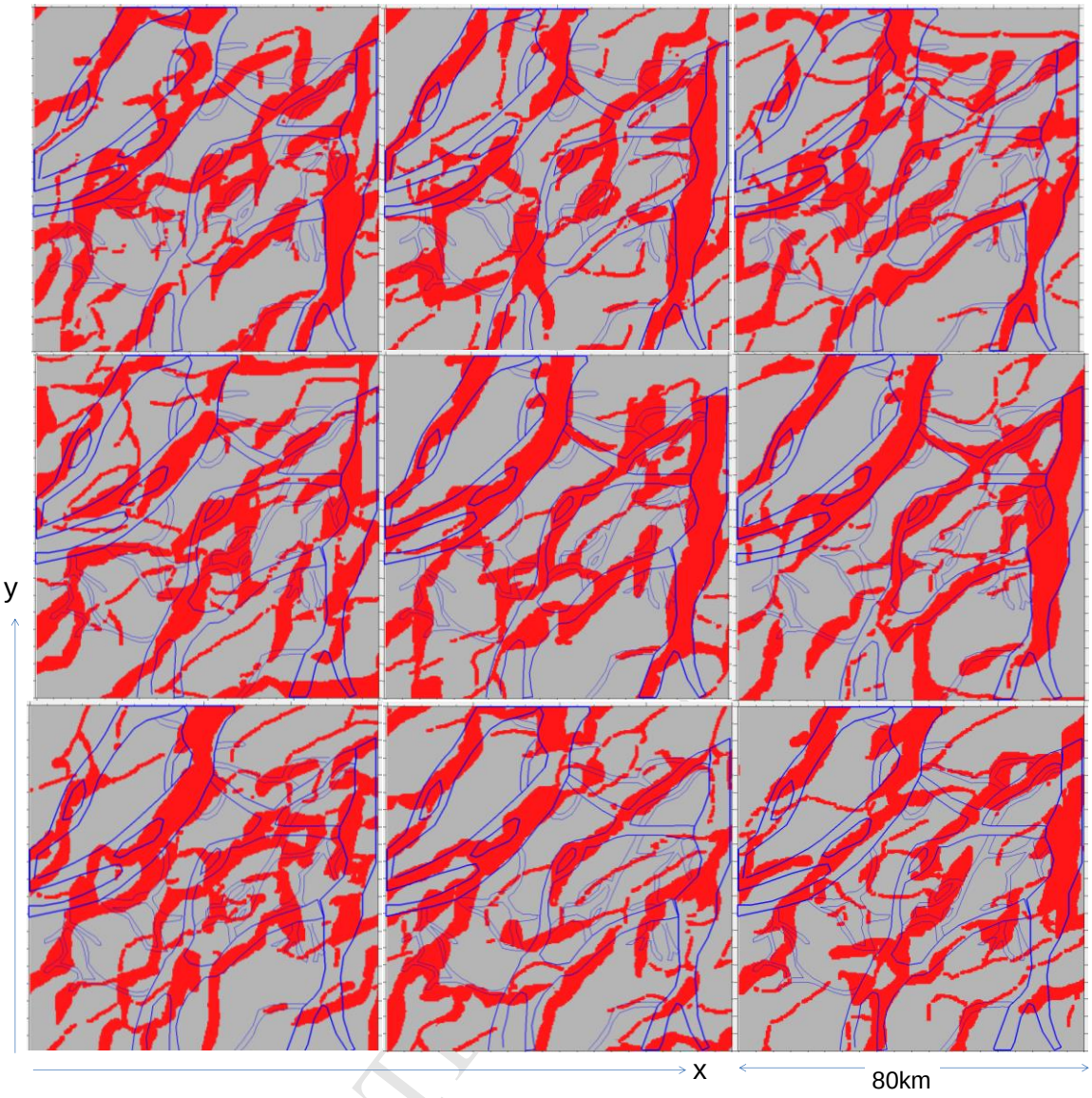

Fig. 15. Outlines of real channels overlap nine realisations of channel and floodplain distribution by MPS based on the sampled data with spacing of 5.0 km. Note that the training image is from manual mapped facies as shown Fig. 14b.

Highlights

- Multiple-point statistics is used in reproducing an active river's distribution.
- Sequential indicator simulation, object modelling and multiple-point statistics are compared.
- Two different dense data sets are used in modelling and compared for results.